ACS Sustainable Chemistry & Engineering

pubs.acs.org/journal/ascecg

Research Article

Thermally Insulating Cellulose Nanofiber Aerogels from Brewery Residues

Nadia Ahmadi Heidari, Milad Fathi,* Nasser Hamdami, Hesam Taheri, Gilberto Siqueira, and Gustav Nyström*

Cite This: *ACS Sustainable Chem. Eng.* 2023, 11, 10698−10708

Read Online

ACCESS | Metrics & More | Article Recommendations

ABSTRACT: Brewery spent grain (BSG), the main waste of the brewery industry, is often disposed of or sold as an animal feed at low prices, neglecting the potential for further valorization. In this work, BSG was used for the first time to produce cellulose nanofiber aerogels for green thermal insulating applications. Cellulose nanofibers (CNFs) were extracted from BSG through microfluidization with and without TEMPO-oxidation pretreatment to obtain bio-based building blocks for aerogels. The TEMPO-treated CNFs exhibited a finer diameter (5.4 nm) with a more homogeneous size distribution (2−10 nm) than that of nonoxidized samples. All of the produced aerogels demonstrated low densities (0.009−0.031 g/cm^3), low thermal conductivities (32.3−37.7 mW/mK), and a compressive Young's modulus in the range of 4−311 kPa. Unidirectional freezing and TEMPO-oxidation showed a distinct improvement in the thermal conductivity and mechanical properties of the aerogels compared to the random frozen samples. Specifically, the unidirectional frozen aerogel with the highest investigated CNF concentration of 3 wt % exhibited the lowest thermal conductivity (32.4 mW/mK), highest Young's modulus (311 kPa), and good thermal stability. These results show that the BSG-derived nanocellulose is a valuable resource for producing eco-friendly, biodegradable, and thermally insulating aerogels.

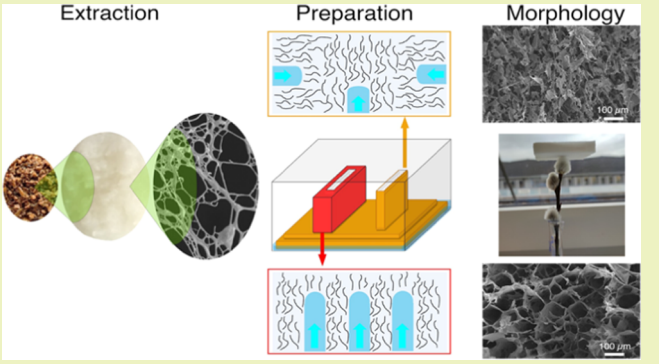

KEYWORDS: *aerogel, cellulose nanofiber, brewery spent grain, thermal insulator, industry waste valorization*

INTRODUCTION

Annually, large amounts of food waste are produced within the supply chain, causing negative economic and ecological effects. The majority of this waste is also forecasted to increase due to both economic and population growth, especially in developing countries.[1] In this respect, beverage industries, especially breweries are major bio-waste producers.[2] The main byproduct of the beer-brewing process (85% w/v) is the so-called brewery spent grain (BSG), which consists of malted grain husks, different layers of the seed coat, and some parts of the pericarp. It has been estimated that the production of every hectoliter of beer generates about 20 kg of wet BSG,[3] leading to total annual residuals of more than 180 million tons worldwide, with 3.4 million tons of residuals being produced annually in Europe alone.[4] While this high volume of low-cost waste is a rich source of fibers (30−50 wt %), proteins (19−30 wt %), polyphenols, vitamins, and antioxidants, it is usually sold as low-value fodder to the animal feed industry or directly disposed of as waste.[5] BSG has a significant role (about 30−60%) in the biochemical oxygen demand (BOD) generation of breweries and is prone to microbial spoilage because of the high amount of water (77−81 wt %) and sugar content, making it a problem from an environmental perspective.[6] Managing and finding ways to valorize this waste is one of the concerns of food industries. In spite of some attempts to reduce waste through bioactive compound extraction for nutraceutical and food concepts, the retained fiber after extraction is still considered waste without any high-value application.[7] BSG can be considered an attractive source of cellulose (16−25 wt %) and nanocellulose materials.[3] Typically, wood is the most common source of cellulose extraction in the industry. However, considering its applications in the construction, furniture, pulp, and paper industries, it is a relatively expensive source.[8] Furthermore, there is a general trend, for CO_2 and sustainability reasons, to keep wood in its solid form and use it in applications for long-term use rather than disintegrating it to its biopolymeric constituents.

Received: March 6, 2023
Revised: June 13, 2023
Published: July 12, 2023

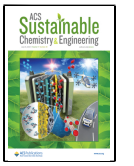

Table 1. Sample Coding of Materials According to the Different Treatments and Processing Methods[a]

sample name	alkaline treatment	bleaching	TEMPO-oxidation	microfluidization	
				5 passes	10 passes
BSG	−	−	−	−	−
BSG-A	+	−	−	−	−
BSG-AB	+	+	−	−	−
BSG-ABM5	+	+	−	+	−
BSG-ABM10	+	+	−	+	+
BSG-ABTM5	+	+	+	+	−

[a]The abbreviations are representative of A: alkaline treatment, B: bleaching, M: microfluidization (5 passes and 10 passes), and T: TEMPO-oxidation.

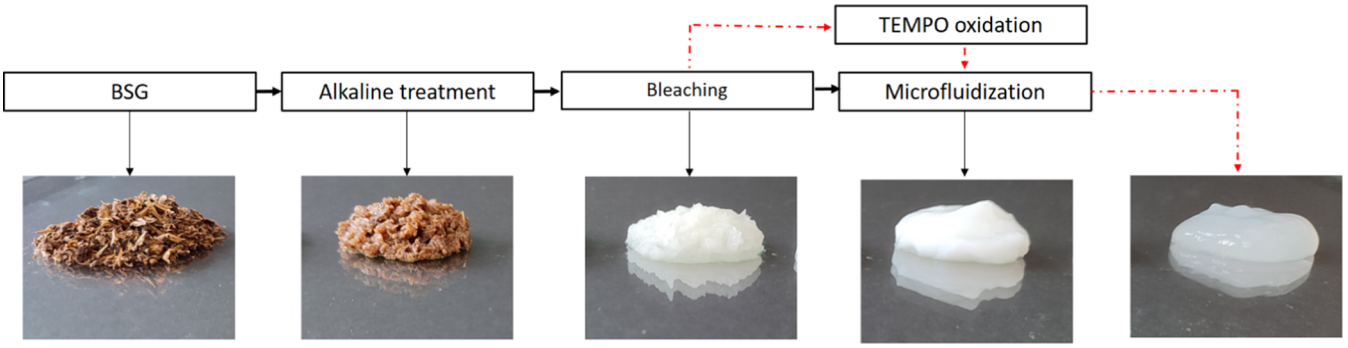

Figure 1. Schematic image of different treatment steps during the CNF extraction (red dashed arrows indicate TEMPO-treated CNF production stages).

Therefore, the focus on using food and agricultural wastes as an alternative source of cellulose extraction has considerably increased in recent years.[9]

Cellulose nanofiber (CNF) is an abundant and natural eco-friendly material with a width range of 5−70 nm and a length between 500 nm and several micrometers.[10] It can be produced at large scales and is used in many different applications. Different methods can be used to extract or produce CNF, including (i) mechanical processing such as grinding,[11] homogenization/microfluidization,[12] and twin-screw extrusion (TSE) methods[13] or (ii) the combination of mechanical processing and chemical/enzymatic treatments such as 2,2,6,6-tetramethylpiperidine-1-oxyl (TEMPO)-mediated oxidation.[14]

CNF has the potential to be used as the building block for multifunctional materials, such as aerogels, whose properties can be tuned by its three-dimensional network structure and its modifiable surface chemistry.[15] Being one of the major classes of biopolymer aerogels,[16] cellulose aerogels may find applications in several disciplines including medicine and tissue engineering,[17] sensors,[18] adsorbents,[19] drug and nutrient delivery,[20] and thermal insulation.[21]

The low thermal conductivity of aerogels can be attributed to their low density and small pore sizes. It is well known that total thermal conductivity in porous materials is the sum of thermal conductivity through solids, gas, and radiation.[22] In solids, conduction decreases thanks to the existence of more air in more porous material structures. Meanwhile, if the pore size is smaller than the mean free path of gas molecules (70 nm), gas thermal diffusion is also hindered.[23] Furthermore, heat transfer through radiation is negligible at room temperature. Recent research has shown that a combination of supercritical drying and material density can be used to tune thermal conductivity to reach super-insulating properties (lambda < 20 mW/mK) at densities of around 65−70 mg/cm^3 in line[24] or at higher densities[25] than those previously reported. Taken together, these properties make it possible to tune the thermal conductivity by both the processing method and material density, thereby making cellulose aerogels promising materials to use as a thermal insulator in food packaging.

Freeze drying and supercritical drying are the most widespread methods of aerogel production. Whereas freeze drying is easier to operate and has the advantage of reducing the need for solvent exchange, the freezing process typically influences the microstructure as well as the resulting physical properties of the porous material. As recent studies have shown, the freezing process can also be used to control the aerogel pore size and distribution by controlling the ice growth rate and direction.[26]

In this work, the potential use of beer industry waste materials as a source of CNF has been explored to produce high-value-added nanocellulose and nanocellulose aerogel materials as thermal insulators in packaging applications. The CNF from beer waste was extracted using microfluidization with and without TEMPO-oxidation pretreatment. The properties of aerogels obtained from the extracted CNF were then compared with respect to the processing method, CNF concentration, and microstructure induced by unidirectional or random freeze casting. Specifically, the morphology, thermal conductivity, mechanical properties, density, porosity, and thermal properties of the resulting aerogels were analyzed.

EXPERIMENTAL SECTION

Materials. BSG was supplied by a local brewery in Dübendorf (Pentabier, Switzerland). Obtained materials were immediately frozen at −21 °C (The dry content of the material was 25.49%). Sodium chlorite (80% purity) and acetic acid were purchased from VWR International Company.

BSG Pretreatment. Two kinds of CNFs were produced through microfluidization independently and in combination with TEMPO-

https://doi.org/10.1021/acssuschemeng.3c01113
ACS Sustainable Chem. Eng. 2023, 11, 10698−10708

Table 2. Sample Coding of Aerogels According to Different Concentrations and Freezing Methods

			concentration (wt %)			freezing method	
sample name	BSG-ABM10	BSG-ABTM5	1	2	3	random directional	unidirectional
aerogel-R1	+	−	+	−	−	+	−
aerogel-R2	+	−	−	+	−	+	−
aerogel-R3	+	−	−	−	+	+	−
aerogel-U1	+	−	+	−	−	−	+
aerogel-U2	+	−	−	+	−	−	+
aerogel-U3	+	−	−	−	+	−	+
aerogel-TU1	−	+	+	−	−	−	+

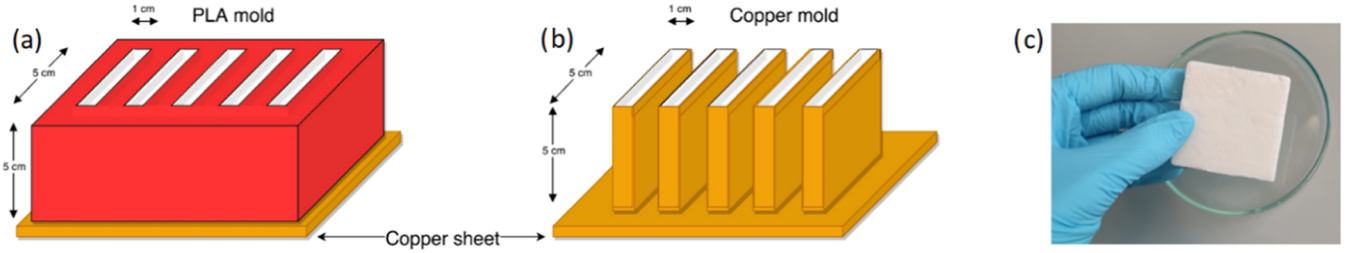

Figure 2. Different molds were used for (a) unidirectional and (b) random freezing. (c) Photograph of Aerogel-TU1.

oxidation to assess the influence of different building blocks on the final aerogel properties (Table 1). The BSG was also pretreated with alkali and bleached before processing according to the Berglund et al. procedure with some modifications,[27] including elimination of the washing stage and reducing the number of bleaching times from three to one.

Alkaline Treatment. For this purpose, frozen BSG was initially defrosted and dispersed (2 wt %) in a sodium hydroxide aqueous solution (2 wt %). The obtained dispersion was treated for 2 h at 80 °C, under gentle agitation (80 rpm) in a glass 10 L reactor with a heating jacket and an electric mixer (LaboTechSystems LTS AG, Reinach, Switzerland). The dark brown slurry obtained from alkaline treatment was filtered and washed several times with distilled water to remove sodium hydroxide completely. Figure 1 illustrates CNF production schematically.

Bleaching. For the next step, the alkaline-treated BSG (2 wt %) was subjected to bleaching with 6 L of a solution consisting of equal volumetric parts of sodium chlorite (1.7 wt %) and acetate buffer. The treatment was carried out for 2 h at 80 °C under gentle agitation in the glass reactor. Once a yellow color was observed in the solution, it was allowed to cool down and was subsequently filtered/washed with distilled water several times to completely remove sodium chlorite. The bleached pulp showed a white color, which was the result of lignin, hemicellulose, pectin, and other impurities removal during the chemical treatments (Figure 1). The calculated yield of extraction based on the dry content of the initial sample was 16.24% ± 2.00.

TEMPO-Oxidation. This treatment was performed based on the procedure described by Saito et al. with minor modifications.[28] First, TEMPO (0.1 mmol/g cellulose) and sodium bromide (1 mmol/g cellulose) were dissolved in distilled water and then added to the cellulose dispersion (1 wt %). The pH was kept at 10−11 by the addition of sodium hydroxide (2 wt %) and after reaching the stable pH, a 14% NaClO solution (10 mmol/g cellulose) was added while stirring at room temperature. The reaction continued for 2 h after adding the whole NaClO solution. Finally, the TEMPO-oxidized cellulose was filtered and completely washed with distilled water until the conductivity reached less than 100 μS/cm.

CNF Extraction. The treated/bleached and TEMPO-oxidized BSG was microfluidized to prepare the CNF suspension. A concentration of 1 wt % of each sample as shown in Table 1 was prepared and completely mixed by an Ultra-Turrax for 15 min at 10,000 rpm (Ultra-Turrax T25, IKA GmbH & Co, Staufen, Germany) prior to microfluidization. The bleached sample was then passed through a microfluidizer (8 bar, M110Y, Microfluidics Corporation, Newton, Massachusetts) for 10 passes. For the primary 5 passes, 400 and 200 μm interaction chambers were used and the operation was continued for the secondary 5 passes with 200 μm and 100 μm chambers. For the TEMPO-oxidized fibers, the Ultra-Turrax mixing was omitted and the sample only received 5 passes of microfluidization in the 200 and 100 μm chambers. BSG-ABM10 had a milky appearance, while BSG-ABTM5 showed a transparent appearance and higher viscosity (Figure 1).

Aerogel Preparation. Samples were prepared using freeze casting and subsequent freeze drying. The obtained porous materials, which based on the preparation method could also be classified as cryogels or xerogels, are here referred to using the general term aerogels. To compare the effect of the different building blocks and freezing methods on the aerogel properties, aerogels were prepared using freeze casting and subsequent freeze drying from BSG-ABM and BSG-ABTM5 (Table 2) using two kinds of molds, as shown in Figure 2, promoting unidirectional or random microstructures.

For the preparation, BSG-ABM in concentrations of 1, 2, and 3 wt % was poured into the unidirectional and random molds, and the whole molds were placed in a polystyrene box to add liquid nitrogen. The level of liquid nitrogen was kept constant over a total freezing period of 20 min. Different aerogels from BSG-ABM10 were prepared via both freezing methods. From the TEMPO-treated sample, BSG-ABTM5, only aerogels by the unidirectional freezing method were prepared.

Characterization. To study the BSG structure before and after different treatments, optical microscopy (Zeiss Axioplan, Germany) was used. Dilution in water to 0.01 wt % was performed prior to the investigation. Scanning electron microscopy (SEM, Fei Nova NanoSEM 230) was used to study the microstructures of CNFs and aerogels at an acceleration voltage of 5 kV. For CNF samples, dilution in water to 0.01 wt % was carried out. Samples were clamped on sample holders and the coating was done with a thin layer of platinum (7 nm). Aerogel samples were frozen in liquid nitrogen and then broken into small pieces, which were clamped on the sample holder and coated with platinum. Atomic force microscopy (AFM, Bruker Icon 3 equipped with Bruker RTESPA-150 probes) in tapping mode was used for further evaluation of fibrillation. BSG-ABM10 and BSG-ABTM5 were first diluted in MilliQ water (0.001 wt %). Mica was then modified by pouring 0.05 wt % (3-aminopropyl)-triethoxysilane (APTES) and drying with pressured air to create a positive charge and better deposition of negatively charged CNFs. A drop of a diluted CNF suspension was poured on mica and investigated after drying. ζ-Potential measurement carried out for

https://doi.org/10.1021/acssuschemeng.3c01113
ACS Sustainable Chem. Eng. 2023, 11, 10698−10708

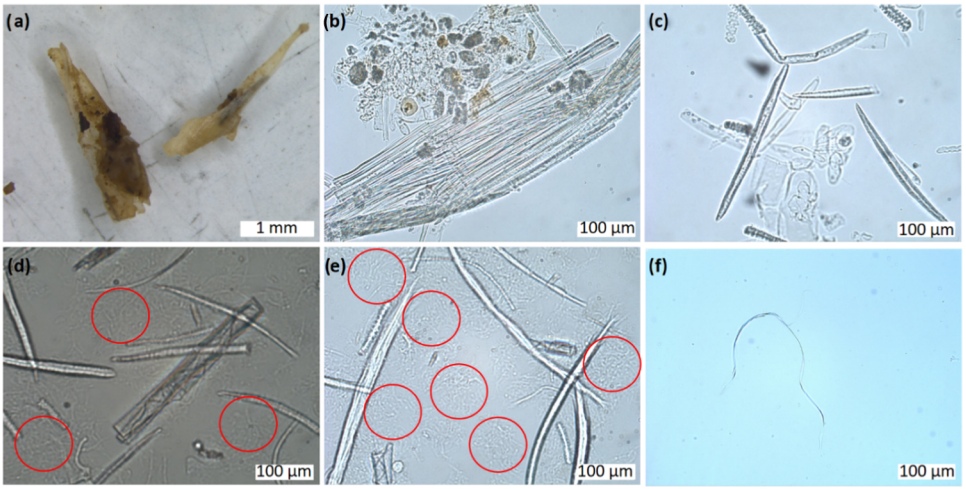

Figure 3. Optical microscopy images of (a) BSG, (b) BSG-A, (c) BSG-AB, (d) BSG-ABM5, (e) BSG-ABM10, and (f) BSG-ABTM5 (Table 1).

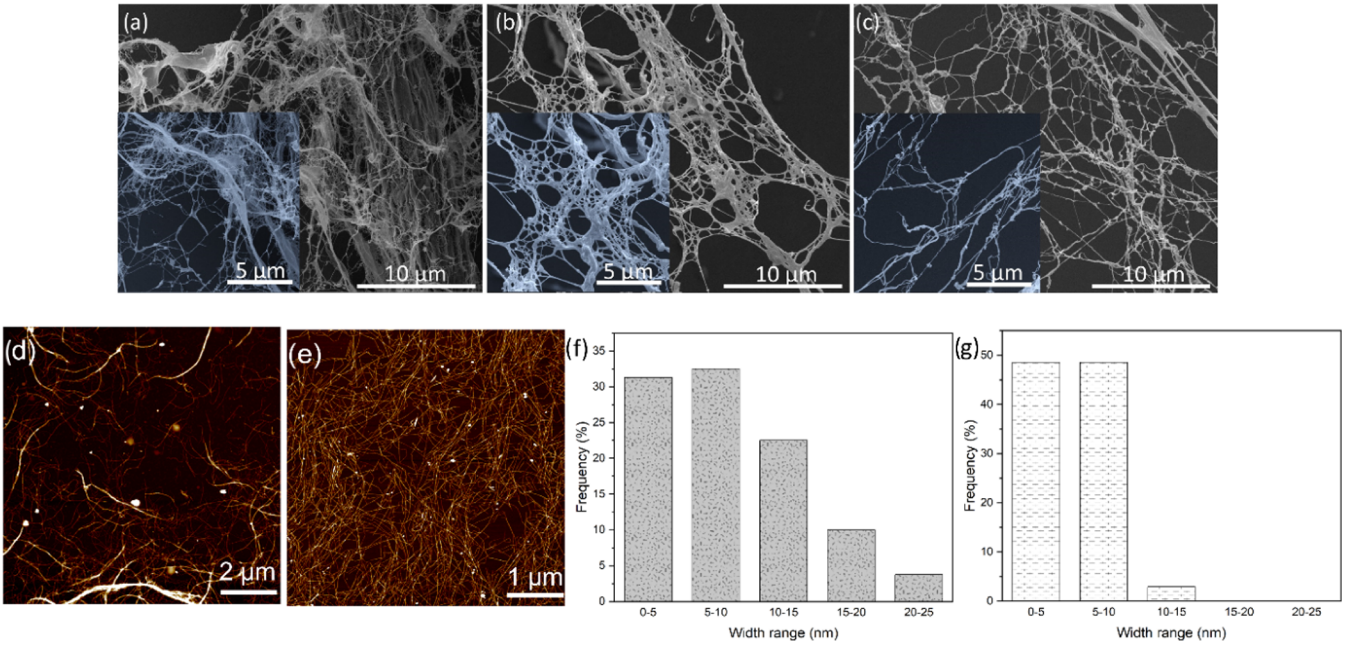

Figure 4. SEM and AFM images and diameter distribution of (a) BSG-ABM5, (b, d, f) BSG-ABM10, and (c, e, g) BSG-ABTM5, respectively. The inset images show higher magnifications.

stability evolution of the CNF dispersion by a Zetasizer Nano ZS (Malvern, U.K.) at a wavelength of 633 nm and a detection angle of 173°. A dispersion of 0.01 wt % BSG-ABM10 and BSG-ABTM5 in 10 mM NaCl was prepared and samples were sonicated (5 min) before testing. All of the measurements were done at 25 °C. XRD patterns after each treatment have been analyzed with a PANAlytical lMPD instrument using a Bragg−Brentano setup to determine the effect of treatments on the crystalline structure of samples. Data collection was performed at room temperature using Cu Kα radiation (λ = 1.5406 Å) in the 2θ range of 2−100°. The crystallinity (%) of a sample is defined by the area ratio of the crystalline peaks and the sum of all measured area (eq 1)[29]

$$\text{crystallinity (\%)} = 100 \times \frac{A_C}{A_C + A_a} \quad (1)$$

where A_C and A_a represent the total crystalline peak area and the total amorphous peak area, respectively.

Fourier transform infrared spectroscopy (FTIR, Bruker Tensor 27 FTIR spectrometer, Switzerland) with a ZnSe crystal attenuated total reflectance (ATR) cell was run to explore chemical composition changes after each treatment. The wavenumber range of 400−4000 cm^{-1} with a resolution of 4 cm^{-1} and 32 scan rate was used for the examination of freeze-dried samples. The steady-state shear viscosity as a function of shear rate was measured to study the flow properties of CNF suspensions. An aqueous dispersion of BSG-ABM5, BSG-ABM10, and BSG-ABTM5 at 1 wt % was prepared. Measurements were performed at 23 °C with a Physica MCR 302 rheometer (Anton Paar) equipped with a cone-plate geometry (d = 2.5 cm, angle of 2.008°) and an operation gap of 0.105 mm. The applied shear rate ranged between 0.01 to 100 s^{-1} and data were collected over 20 min. In order to avoid undesirable shear effects during the sample loading, it was rested for 5 min before starting the test. The standard hood cover was used to avoid water evaporation overall measurements.

The porosity of the aerogels was calculated according to the following equation

$$\text{porosity} = \left(1 - \frac{\rho_b}{\rho_s}\right) \times 100 \quad (2)$$

https://doi.org/10.1021/acssuschemeng.3c01113
ACS Sustainable Chem. Eng. 2023, 11, 10698−10708

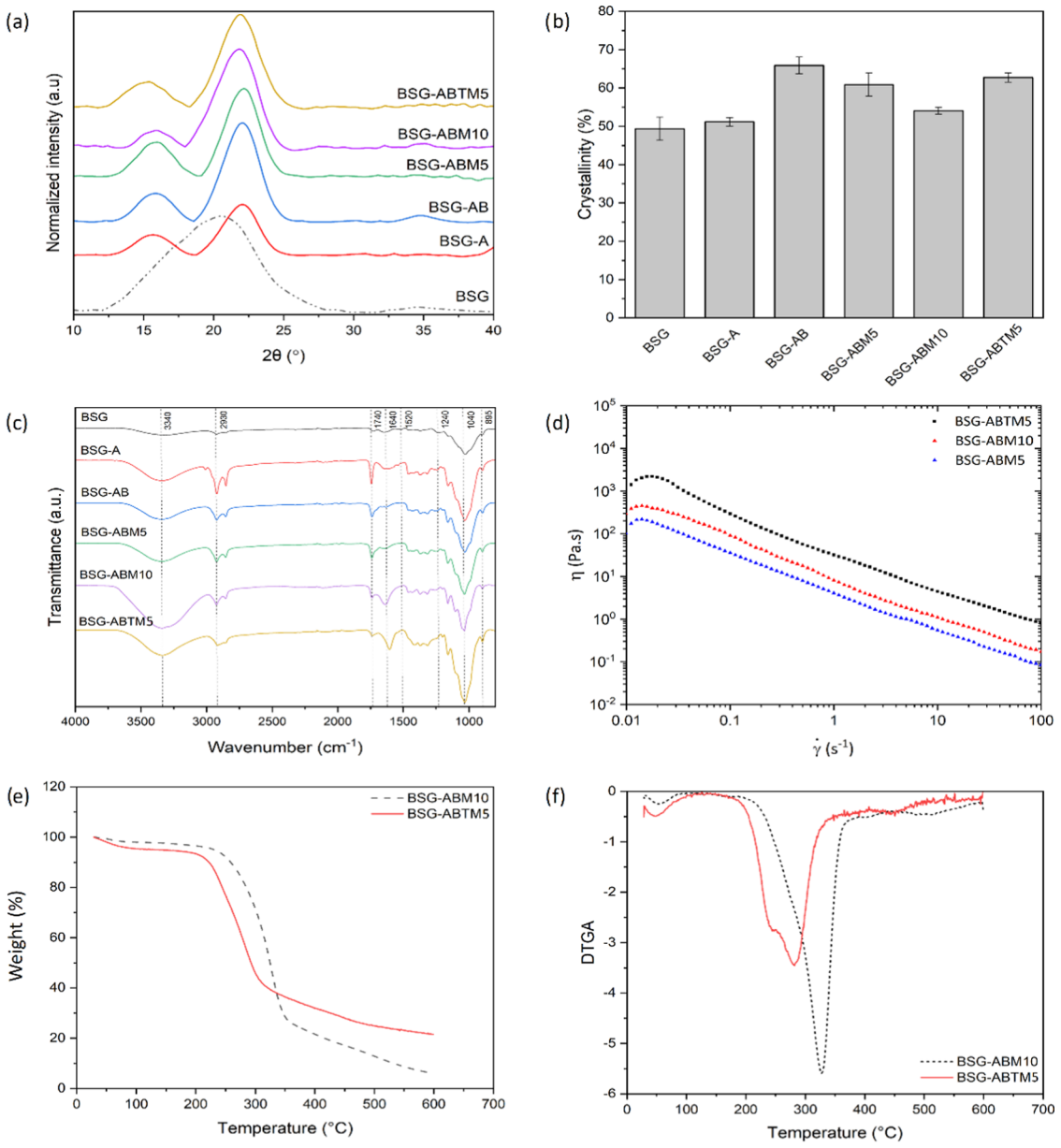

Figure 5. (a) XRD patterns, (b) percent of crystallinity, and (c) FTIR spectra of BSG after each treatment step; (d) shear viscosity behavior of BSG-ABM5, BSG-ABM10, and BSG-ABTM5 (1 wt %) at 23 °C; and (e) TGA and (f) differential thermogravimetric (DTGA) curves of BSG-ABM10 and BSG-ABTM5 (Table 1).

where ρ_b is the bulk density of the aerogel and ρ_s represents the skeletal density of cellulose (1.5 g/cm^3). The average and standard deviation were determined through triplicate measurements. A compression test was carried out to investigate the effect of CNF types and freezing methods on the mechanical properties of aerogels. For this purpose, cubic samples with a width/height ratio of 1:3 and a thickness range of 0.8−1 cm were prepared. A universal testing machine (Zwick 1484, Zwick GmbH, Germany) with a 100 N load cell and a speed of 1 mm/min was used. Preload was set at 0.1 N with a speed of 5 mm/min. At least five measurements for each sample were performed. Thermogravimetric analysis (TGA) was conducted to study the thermal properties of CNFs and aerogels using a Netzsch TG 209F1 thermogravimetric analyzer. The measurements were carried out under a nitrogen atmosphere by heating the samples from room temperature to 600 °C at a heating rate of 5 °C/min. Thermal conductivity data were collected through a special lab-scale device equipped with a hot plate at the upper part (30 °C) and a cooling unit at the bottom (20 °C). Samples with dimensions of 50 mm × 50 mm × 10 mm were put between two plates and a unidirectional heat flow was generated by an electric heater with a constant heating rate, which passed through the sample. The temperature difference over the sample was caused by heat flow and served as the measure of its thermal conductivity. Measurement was performed for a total run time of 45 min and thermal conductivity was calculated by measuring the steady-state heat flow and correction factors.[30] The mean thermal conductivities with standard deviation were presented for triplicate measurements.

RESULTS AND DISCUSSION

BSG-ABM and BSG-ABTM5 cellulose nanofibers were extracted from the industrial beer waste using alkaline, bleaching, and microfluidization treatment independently or in combination with TEMPO-oxidation. The fibrillation of cellulose fibers during the different steps of the process was investigated by optical microscopy. The raw BSG possessed a tough and rigid structure. As shown in Figure 3a, it had a

https://doi.org/10.1021/acssuschemeng.3c01113
ACS Sustainable Chem. Eng. 2023, 11, 10698−10708

particle size of several millimeters before and alkaline treatment converted it into microsized bundle structures (Figure 3b). Lignin acts as an adhesive between cellulose fibers, but bleaching can break down these adhesive bonds, resulting in water-soluble components.[31] As can be seen in Figure 3c, bundle structures disappeared after bleaching. Moreover, with the use of microfluidization, several microscale fibers can still be observed and, significantly, some agglomerated regions appeared in the image background (marked with red circles) with their number increasing after 10 passes. The presence of these regions might be a sign of nanofiber formation (Figure 3d,e). Few visible structures were observed for the combination of TEMPO and microfluidization (Figure 3f), indicating a well-fibrillated material with a predominant material fraction in the nanoscale.

To further elucidate the materials' morphology, the cellulose nanofibers were also investigated by SEM (Figure 4). A comparison of the SEM of BSG-ABM5, BSG-ABM10, and BSG-ABTM5 confirmed that five microfluidization cycles were not enough to achieve complete fibrillation of the samples without TEMPO-oxidation (Figure 4a), while BSG-ABM10 showed a web-like structure and complete fibrillation (Figure 4b). Furthermore, the combination of TEMPO-oxidation and microfluidization resulted in finer fibrils (Figure 4c), likely as a result of the carboxyl groups on the surface of these CNFs, which are well known to facilitate fiber individuation due to the charge-induced repulsive forces between the CNFs.

Figure 4d,e shows the AFM images of BSG-ABM10 and BSG-ABTM5. From the AFM images, produced CNFs exhibited long and entangled structures, making estimation of the exact length of nanofibers impossible. However, their average diameters could be estimated based on the height data from AFM by measuring at least 50 fibers. It was found that the BSG-ABM sample contained two groups of fibrils: thicker fibrils with an average diameter of 16.1 nm and finer fibrils with an average size of 5.7 nm (Figure 4f). TEMPO-treated CNF possessed a finer diameter with an average size of 5.4 nm and a completely homogeneous size distribution (Figure 4g).

The ζ-potential is a key parameter in determining the suspension stability of CNFs and gives a representation of the surface charge and repulsion degree between the fibers. Good suspension stability of the CNFs is desirable for producing well-structured aerogels. It has been reported that suspensions with ζ-potentials of less than −30 mV have good stability.[32] Highly negative ζ-potential values lead to more repulsive forces between the similarly charged fibers and consequently help to prevent fiber aggregation.[33] The average ζ-potential of BSG-ABM10 was −27.9 mV, which was lower than BSG-ABTM5's average ζ-potential of −48.16 mV. The greater absolute value of the ζ-potential of the BSG-ABTM5 sample originated from the TEMPO-oxidation treatment's introduction of a negatively charged carboxyl group over the cellulose surface.

X-ray diffraction (XRD) patterns of raw and treated BSG are shown in Figure 5a. Raw BSG exhibited a broader peak than treated samples and had its main peak at around 2θ = 20.5°. Two peaks around 2θ = 16 and 22° were observed for treated samples, which were typical of cellulose I[34] and became more clear after chemical treatments and the removal of impurities. The crystallinity index (CI) of the samples is presented in Figure 5b. The CI increased continuously by chemical treatments, indicating the elimination of disordered parts by applied treatments. A small decrease in crystallinity was observed after mechanical treatment. It has been reported that intense mechanical processing can break down crystalline cellulose structures due to high frictional and shear forces, leading to decreasing CI.[35] In one of the few studies done on BSG nanofibers, the CI of raw, alkaline, and bleached BSG was calculated to be 27.3, 46.7, and 56.5%, respectively.[36]

In order to track the chemical changes of BSG after each treatment, FTIR analysis was conducted. FTIR spectra of the raw and treated BSG are shown in Figure 5c. The bands near 3340 and 2930 cm^{-1} represented the stretching vibrations of O−H and C−H groups in cellulose, respectively.[37] The peaks around 1040 and 895 cm^{-1} corresponded to the C−O stretching and C−H vibrations of cellulose, respectively, which increased after chemical treatments.[36] Another peak at 1640 cm^{-1} was associated with absorbed water.[38] The peak in 1740 cm^{-1} was ascribed to the ester and acetyl groups of hemicellulose or carbonyl groups in the lignin structure[39] or COO groups after oxidation. The small shoulders at 1520 and 1240 cm^{-1} in the spectrum of raw BSG can be attributed to C═C in the aromatic rings and aryl−alkyl ether groups of lignin, respectively.[39] The peak at 1520 disappeared after bleaching, indicating the successful removal of lignin.

Figure 5d represents the flow properties of BSG-ABM5, BSG-ABM10, and BSG-ABTM5 at a concentration of 1 wt %. Rheological measurement provides better insights into the degree of fibrillation in the bulk state. Fiber size and homogeneity, aspect ratio, fibrillation degree, and surface chemistry are the main factors affecting CNF flow behavior. BSG-ABTM5 exhibited higher viscosity and yield stress due to its higher surface charge. It has been argued that by increasing surface charge, shear viscosity increases. Higher charge density leads to higher fibrillation levels and consequently higher surface area, which can adsorb more water and provide more robust network structure formation.[40] Furthermore, BSG-ABM10 showed higher viscosity than BSG-ABM5 due to its higher degree of mechanical fibrillation. Optical microscopy and SEM images clearly supported the obtained data from the shear viscosity test. The rheological data further indicates that all samples showed shear-thinning behavior that can be attributed to network disruption and interaction breakdown of nanofibers due to the applied shear stress.

The TGA and DTGA curves of BSG-ABM10 and BSG-ABTM5 are shown in Figure 5e,f. The obtained results revealed that the CNF dimension and preparation method significantly affected the thermal stability of CNF. The TEMPO-treated CNF showed lower thermal stability due to its smaller dimension and higher amounts of the carboxylic group. The initial weight loss (2−5%) for both samples, which started from temperatures below 100 °C, was attributed to the evaporation of adsorbed water.[41] A significant weight loss was observed at temperatures between 200 and 320 °C for BSG-ABTM5 and 200 and 360 °C for BSG-ABM10. This weight loss occurred due to cellulose degradation through dehydration, depolymerization, and secondary bond cleavage mechanisms.[42] The lower thermal degradation at 281.6 °C and higher solid residue (21.55%) at 599.3 °C were observed for BSG-ABTM5, while the thermal degradation peak of BSG-ABM10 was at 327.3 °C with solid residue (6.01%) at 599.3 °C. The lower thermal stability of TEMPO-treated CNF could be attributed to the smaller dimension of BSG-ABTM5, which can result in a higher surface area. Furthermore, it has been reported that the carboxyl content of cellulose can affect the thermal stability of CNF. For instance, CNFs from different sources with similar carboxylic group content showed similar

https://doi.org/10.1021/acssuschemeng.3c01113
ACS Sustainable Chem. Eng. 2023, 11, 10698−10708

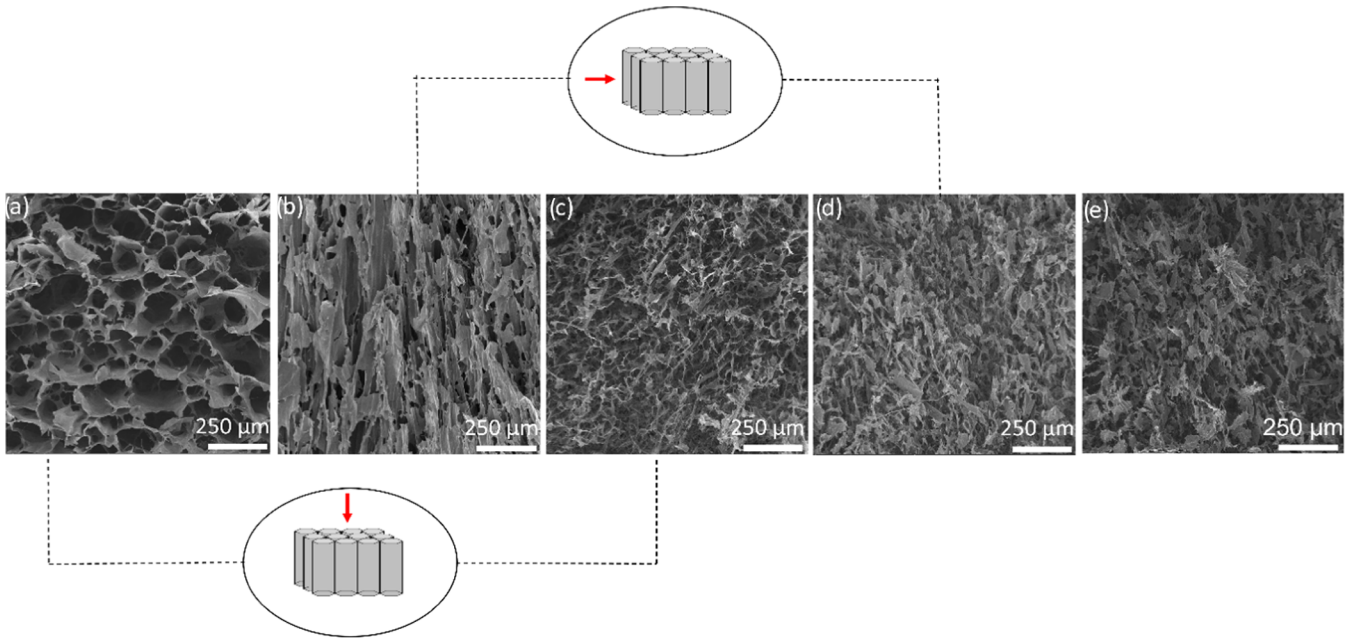

Figure 6. SEM images of Aerogel-TU1, perpendicular to cross section (a) and in the longitudinal direction (b). Aerogel-U3, perpendicular to the cross section (c) and in the longitudinal direction (d). Aerogel-R3 in both directions (e).

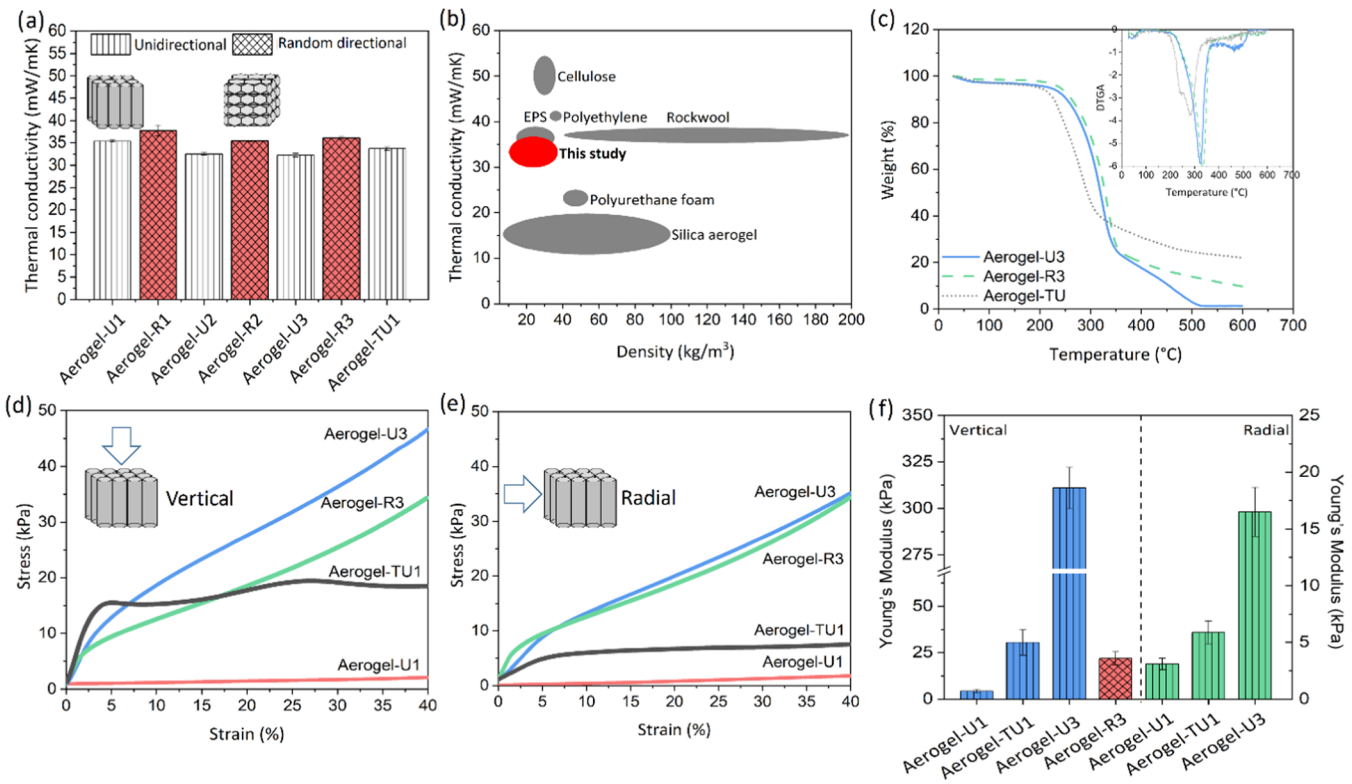

Figure 7. (a) Thermal conductivity of aerogels with different concentrations and freezing methods (Table 2). (b) Thermal conductivity versus density of conventional thermal insulators and silica aerogel[53] in comparison with the current study. (c) TGA and DTGA curves of Aerogel-U3, Aerogel-R3, and Aerogel-TU1. (d) Stress−strain curves of aerogels in vertical and (e) radial directions. (f) Young's modulus of the aerogels in both vertical and radial directions.

thermal stability.[43] It has been argued that decarbonation of anhydroglucuronic acid units, formed during the TEMPO treatment, decreases the thermal stability of TEMPO-oxidized CNF.[43] Mahendra et al. obtained lower thermal stability for TEMPO-treated CNF in comparison with α-cellulose.[44] They interpreted that TEMPO-oxidation might reduce the polymerization degree of cellulose, leading to molecular weight reduction and thermal decomposition, therefore, occurring at lower temperatures. Lower thermal stability and a higher residue amount (28%) were reported for TEMPO-treated CNFs.

https://doi.org/10.1021/acssuschemeng.3c01113
ACS Sustainable Chem. Eng. 2023, 11, 10698−10708

The microstructure of the obtained aerogels was investigated by SEM (Figure 6). The freezing methods (unidirectional and random) were used to manipulate the microstructure and final properties of obtained aerogels. Aerogel-TU1 demonstrated an anisotropic porous structure as a result of following the ice crystal growth direction during unidirectional freezing (Figure 6a). Moreover, the pores showed circular cross sections with thin pore walls. It seems that CNF entanglement restricted large ice crystal growth and lamellar structure formation; therefore, a circular pore shape was formed.[45] The longitudinal view of Aerogel-TU1 also showed an oriented layered structure toward the direction of ice crystals' growth (Figure 6b). Aerogel-U3 showed a denser structure with a smaller pore size (Figure 6c). Unlike Aerogel-TU1, oriented pores can hardly be observed in the cross section of Aerogel-U3. The reason should be explored in different CNF dimensions and concentrations used to produce these two aerogels. The CNF produced via a microfluidizer and used in Aerogel-U3 had a greater fiber diameter, which restricted the fiber diffusion due to the higher weight. Moreover, the microfluidized CNF dispersion with a concentration of 3 wt % exhibited lower flow ability than a 1 wt % TEMPO-treated CNF dispersion. Therefore, the fibers' rotational freedom was restricted, and consequently, the structure will not be consistently generated with ice crystals' growth (Figure 6d). Aerogel-R3 showed a similar dense structure in both directions (Figure 6e).

All of the produced aerogels exhibited low densities in the range of 0.009−0.030 g/cm^3 and high porosity from 97.92 to 99.35%. Similar results were also reported by several researchers.[46−48]

The thermal insulation performance of the produced aerogels is presented in Figure 7a, ranging from 32.3 to 37.7 mW/mK. The obtained thermal conductivities for the samples were better than or in the range of alginate-CNF aerogel (31.5 and 34.8 mW/mK), polyamide-bacterial cellulose aerogel (23−44 mW/mK), and starch-clay aerogel (41.5−48.3 mW/mK), which also used freeze drying.[49−51] Supercritical drying, which has also often been used, generates smaller pore sizes and consequently lower thermal conductivity. The total thermal conductivity of a porous material is the sum of thermal conductivity through the solid backbone, gas phase, and radiation. By decreasing the pore size, heat transfer through the gas phase (thermal convection) decreases, leading to diminishing total thermal conductivity. Figure 7b shows a comparison between the thermal conductivity of produced aerogels and traditional thermal insulation materials as a function of density. As can be seen in the figure, the obtained aerogels showed comparable thermal conductivity values to EPS, rock wool, polyethylene, and loose-fill cellulose.

Regardless of the preparation method, increasing the concentration led to an increasing density. The thermal conductivity of the aerogels decreased as a result of the smaller pore size and higher tortuosity of the solid paths. On the other hand, the thermal conductivity of unidirectional freezing samples was measured in the longitudinal direction and all of the unidirectional freezing aerogels showed lower thermal conductivity than their corresponding random counterparts. Thermal gas convection in the radial direction was restricted in the unidirectional frozen tubular structure, which led to a reduction of heat propagation through the gas phase. Moreover, the heat transfer via thermal radiation was reduced as a result of several emissions and refractions between the walls. Both of them led to lower thermal conductivity of unidirectional samples than that of random samples.

By comparing the thermal conductivity of the samples at a concentration of 1 wt %, it can be seen that Aerogel-TU1 exhibited lower thermal conductivity (33.7 mW/mK) than Aerogel-U1 (35.36 mW/mK) and Aerogel-R1 (37.73 mW/mK). Since Aerogel-TU1 and Aerogel-U1 had similar concentrations and freezing methods, it can be concluded that TEMPO-oxidation could improve the thermal insulation performance of the obtained aerogel. Figure 7c represents the thermal properties of produced aerogels. Aerogel-U3 and Aerogel-R3 showed three weight losses by increasing temperature, while Aerogel-TU1 exhibited four steps. The first negligible weight loss, 1−3%, in all of the samples occurred around 100 °C and corresponded to water evaporation, which is a common phenomenon in hydrophilic samples like cellulose. The second weight loss, around 80%, for Aerogel-U3 and Aerogel-R3 was observed at 200−380 °C with a degradation peak at around 320−330 °C. This weight loss was ascribed to the degradation of polymer chains. Aerogel-TU1 demonstrated two main degradation peaks around 240 and 280 °C with 18.58 and 41.46% weight losses, respectively. The lower degradation peak of Aerogel-TU1 than those of Aerogel-U3 and Aerogel-R3 might be the result of cellulose degradation and decarboxylation of sodium anhydroglucronate units during the TEMPO-oxidation, which is in agreement with previous studies.[52] Moreover, Aerogel-TU1 demonstrated a higher amount of retained char (21.55%) at 600 °C, while it was about 9.79 and 1.35% for Aerogel-R3 and Aerogel-U3, respectively. Overall, it seems that unidirectional or random freezing did not have a significant effect on the thermal stability of produced aerogels, since Aerogel-U3 and Aerogel-R3 showed approximately similar thermal degradation trends. In contrast, the chemical treatment of CNF was more effective on the thermal stability of the aerogel such that Aerogel-TU1 exhibited lower thermal stability with a higher amount of residue.

Four aerogels with different concentrations (1 and 3 wt %) and freezing methods were selected to verify the effect of concentration and unidirectional/random freezing on the mechanical properties of aerogels. Figure 7d,e represents the strain−stress curves of aerogels in vertical and radial directions, respectively. Moreover, Young's modulus (Figure 7f) calculated from the slope of the linear part at 0−2% strain (Figure 7d,e) was used to compare the mechanical properties of the samples. As shown in Figure 7d,e, by increasing the CNF concentration, mechanical strength increased as a result of forming a denser structure, which was more resistant to collapse. Unidirectional freezing had a distinct effect on improving the mechanical properties, for instance, the Young's modulus of Aerogel-U3 (311 kPa) in the vertical direction was higher than that of Aerogel-R3 (21.93 kPa), corresponding to a 174% increase. The lower mechanical strength of Aerogel-R3 is attributed to the disordered orientation of pores in the structure. Furthermore, all of the unidirectional freezing samples exhibited higher Young's modulus in the vertical than that in the radial direction. The pore wall alignment is the main reason for higher mechanical strength in the vertical direction. Overall, the combination of higher concentration and unidirectional freezing led to more mechanical resistance of Aerogel-U3 than those of the other samples. It is noteworthy to consider the effect of TEMPO-oxidation on the mechanical improvement of the obtained aerogels. By comparing the

https://doi.org/10.1021/acssuschemeng.3c01113
ACS Sustainable Chem. Eng. 2023, 11, 10698−10708

Young's modulus of Aerogel-U1 with that of Aerogel-TU1, a considerable enhancement from 4.33 to 30.5 kPa (about 7-fold) can be detected. Moreover, Aerogel-TU1 demonstrated even better mechanical properties than Aerogel-R3 with a higher concentration. It can be concluded that the smaller building blocks that were used to produce Aerogel-TU1 facilitated better fiber alignment with ice crystal growth during the unidirectional freezing and led to the formation of a more robust structure in the vertical direction.

CONCLUSIONS

In this work, extracted CNF (TEMPO and non-TEMPO) from industrial waste BSG was used to produce CNF aerogels with low thermal conductivity, low density, and desirable mechanical properties by different freezing methods. Although both CNFs demonstrated nanometric size, TEMPO-treated CNF exhibited a finer diameter (5.4 nm) with a more homogeneous size distribution, which produced a more positive effect on the final properties of the produced aerogels. The smaller size of TEMPO-treated CNF made fibril alignment more convenient during the unidirectional freezing. Therefore, the unidirectional frozen aerogel from TEMPO-treated CNF showed an anisotropic porous structure with a circular cross section that resulted in lower thermal conductivity and higher mechanical strength than those of the other aerogels at the same concentration. The effectiveness of TEMPO-treated CNF used in combination with unidirectional freezing on thermal conductivity and mechanical strength became clearer by comparing the thermal conductivity (33.7 mW/mK) and Young's modulus (30.5 kPa) of the unidirectional frozen aerogel (1 wt %) with those of the random frozen aerogel (36.06 mW/mK and 21.93 kPa, respectively) with a higher concentration (3 wt %). However, the lowest thermal conductivity (32.27 mW/mK) and the highest Young's modulus (311 kPa) were observed for the unidirectional frozen aerogel with 3 wt % non-TEMPO-treated CNF. Finally, this study highlighted that brewery industry waste can be considered a good and cheap source of CNF extraction for producing high-added-value aerogels with a facile, eco-friendly procedure without adding any harmful chemicals. The produced aerogels can be used as a bio-friendly insulator in the food packaging of temperature-sensitive materials like meat. This approach not only is advantageous from an environmental perspective but also has potential economic benefits, especially when combined with energy-efficient processing.[54]

AUTHOR INFORMATION

Corresponding Authors

Milad Fathi − *Department of Food Science and Technology, College of Agriculture, Isfahan University of Technology, Isfahan 84156-83111, Iran*; Email: mfathi@cc.iut.ac.ir

Gustav Nyström − *Laboratory for Cellulose & Wood Materials, Empa—Swiss Federal Laboratories for Materials Science and Technology, 8600 Dübendorf, Switzerland; Department of Health Science and Technology, ETH Zürich, 8092 Zürich, Switzerland;* orcid.org/0000-0003-2739-3222; Email: Gustav.Nystroem@empa.ch

Authors

Nadia Ahmadi Heidari − *Department of Food Science and Technology, College of Agriculture, Isfahan University of Technology, Isfahan 84156-83111, Iran; Laboratory for Cellulose & Wood Materials, Empa—Swiss Federal Laboratories for Materials Science and Technology, 8600 Dübendorf, Switzerland*

Nasser Hamdami − *Department of Food Science and Technology, College of Agriculture, Isfahan University of Technology, Isfahan 84156-83111, Iran;* orcid.org/0000-0001-8491-857X

Hesam Taheri − *Laboratory for Cellulose & Wood Materials, Empa—Swiss Federal Laboratories for Materials Science and Technology, 8600 Dübendorf, Switzerland; Université de Bretagne Sud, UMR CNRS 6027, IRDL, 56321 Lorient, France;* orcid.org/0000-0002-5508-5609

Gilberto Siqueira − *Laboratory for Cellulose & Wood Materials, Empa—Swiss Federal Laboratories for Materials Science and Technology, 8600 Dübendorf, Switzerland;* orcid.org/0000-0001-9090-8116

Complete contact information is available at: https://pubs.acs.org/10.1021/acssuschemeng.3c01113

Notes

The authors declare no competing financial interest.

ACKNOWLEDGMENTS

The authors would like to thank Anja Huch for SEM imaging and Beatrice Fischer for TGA. Nico Kummer, Xavier Aeby, and Kevin De France are acknowledged for assistance with AFM, mold preparation, and FTIR, respectively, while Tingting Wu and Deeptanshu Sivaraman are acknowledged for valuable discussions. Kealie Vogel is acknowledged for helping to proofread and language edit the manuscript. The authors acknowledge support from the Federal Commission for Scholarships for Foreign Students for the Swiss Government Excellence Scholarship (ESKAS No. 2021.0924) for the academic years 2021−2022 (awarded to Nadia Ahmadi Heidari). The authors would also like to thank Iran National Science Foundation (grant number of 98016031) and Isfahan Science and Technology Town (ISTT) for their financial support.

REFERENCES

(1) Caldeira, C.; De Laurentiis, V.; Corrado, S.; van Holsteijn, F.; Sala, S. Quantification of Food Waste per Product Group along the Food Supply Chain in the European Union: A Mass Flow Analysis. *Resour., Conserv. Recycl.* **2019**, *149*, 479−488.

(2) Russ, W.; Schnappinger, M. Waste Related to the Food Industry: A Challenge in Material Loops. In *Utilization of by-products and treatment of waste in the food industry*; Springer, 2007; pp 1−13.

(3) Mussatto, S. I.; Dragone, G.; Roberto, I. C. Brewers' Spent Grain: Generation, Characteristics and Potential Applications. *J. Cereal Sci.* **2006**, *43*, 1−14.

(4) Bonifácio-Lopes, T.; Vilas-Boas, A.; Machado, M.; Costa, E. M.; Silva, S.; Pereira, R. N.; Campos, D.; Teixeira, J. A.; Pintado, M. Exploring the Bioactive Potential of Brewers Spent Grain Ohmic Extracts. *Innovative Food Sci. Emerging Technol.* **2022**, No. 102943.

(5) Lynch, K. M.; Steffen, E. J.; Arendt, E. K. Brewers' Spent Grain: A Review with an Emphasis on Food and Health. *J. Inst. Brew.* **2016**, *122*, 553−568.

(6) Naibaho, J.; Butula, N.; Jonuzi, E.; Korzeniowska, M.; Laaksonen, O.; Föste, M.; Kütt, M.-L.; Yang, B. Potential of Brewers' Spent Grain in Yogurt Fermentation and Evaluation of Its Impact in Rheological Behaviour, Consistency, Microstructural Properties and Acidity Profile during the Refrigerated Storage. *Food Hydrocolloids* **2022**, *125*, No. 107412.

(7) Gomez, B.; Miguez, B.; Veiga, A.; Parajo, J. C.; Alonso, J. L. Production, Purification, and in Vitro Evaluation of the Prebiotic Potential of Arabinoxylooligosaccharides from Brewer's Spent Grain. *J. Agric. Food Chem.* **2015**, *63*, 8429−8438.
(8) Blanco, A.; Monte, M. C.; Campano, C.; Balea, A.; Merayo, N.; Negro, C. Nanocellulose for Industrial Use: Cellulose Nanofibers (CNF), Cellulose Nanocrystals (CNC), and Bacterial Cellulose (BC). In *Handbook of Nanomaterials for Industrial Applications*; Elsevier, 2018; pp 74−126.
(9) Motaung, T. E.; Linganiso, L. Z. Critical Review on Agrowaste Cellulose Applications for Biopolymers. *Int. J. Plast. Technol.* **2018**, *22*, 185−216.
(10) Fathi, M.; Karim, M.; Ahmadi, N. Nanostructures of Cellulose for Encapsulation of Food Ingredients. In *Biopolymer Nanostructures for Food Encapsulation Purposes*; Elsevier, 2019; pp 493−519.
(11) Nechyporchuk, O.; Pignon, F.; Belgacem, M. N. Morphological Properties of Nanofibrillated Cellulose Produced Using Wet Grinding as an Ultimate Fibrillation Process. *J. Mater. Sci.* **2015**, *50*, 531−541.
(12) Taheri, H.; Samyn, P. Rheological Properties and Processing of Polymer Blends with Micro-and Nanofibrillated Cellulose. In *Agricultural Biomass Based Potential Materials*; Springer, 2015; pp 259−291.
(13) Ho, T. T. T.; Zimmermann, T.; Hauert, R.; Caseri, W. Preparation and Characterization of Cationic Nanofibrillated Cellulose from Etherification and High-Shear Disintegration Processes. *Cellulose* **2011**, *18*, 1391−1406.
(14) Ho, T. T. T.; Abe, K.; Zimmermann, T.; Yano, H. Nanofibrillation of Pulp Fibers by Twin-Screw Extrusion. *Cellulose* **2015**, *22*, 421−433.
(15) De France, K.; Zeng, Z.; Wu, T.; Nyström, G. Nanocellulose: Functional Materials from Nanocellulose: Utilizing Structure−Property Relationships in Bottom-Up Fabrication. *Adv. Mater.* **2021**, *33*, No. 2170216.
(16) Zhao, S.; Malfait, W. J.; Guerrero-Alburquerque, N.; Koebel, M. M.; Nyström, G. Biopolymer Aerogels and Foams: Chemistry, Properties, and Applications. *Angew. Chem., Int. Ed.* **2018**, *57*, 7580−7608.
(17) Jose, J.; Pai, A. R.; Gopakumar, D. A.; Dalvi, Y.; Ruby, V.; Bhat, S. G.; Pasquini, D.; Kalarikkal, N.; Thomas, S. Novel 3D Porous Aerogels Engineered at Nano Scale from Cellulose Nano Fibers and Curcumin: An Effective Treatment for Chronic Wounds. *Carbohydr. Polym.* **2022**, *287*, No. 119338.
(18) Zhou, S.; Wang, M.; Chen, X.; Xu, F. Facile Template Synthesis of Microfibrillated Cellulose/Polypyrrole/Silver Nanoparticles Hybrid Aerogels with Electrical Conductive and Pressure Responsive Properties. *ACS Sustainable Chem. Eng.* **2015**, *3*, 3346−3354.
(19) Gao, R.; Xiao, S.; Gan, W.; Liu, Q.; Amer, H.; Rosenau, T.; Li, J.; Lu, Y. Mussel Adhesive-Inspired Design of Superhydrophobic Nanofibrillated Cellulose Aerogels for Oil/Water Separation. *ACS Sustainable Chem. Eng.* **2018**, *6*, 9047−9055.
(20) Zhao, J.; Lu, C.; He, X.; Zhang, X.; Zhang, W.; Zhang, X. Polyethylenimine-Grafted Cellulose Nanofibril Aerogels as Versatile Vehicles for Drug Delivery. *ACS Appl. Mater. Interfaces* **2015**, *7*, 2607−2615.
(21) Han, Y.; Zhang, X.; Wu, X.; Lu, C. Flame Retardant, Heat Insulating Cellulose Aerogels from Waste Cotton Fabrics by in Situ Formation of Magnesium Hydroxide Nanoparticles in Cellulose Gel Nanostructures. *ACS Sustainable Chem. Eng.* **2015**, *3*, 1853−1859.
(22) Qu, Z. G.; Fu, Y. D.; Liu, Y.; Zhou, L. Approach for Predicting Effective Thermal Conductivity of Aerogel Materials through a Modified Lattice Boltzmann Method. *Appl. Therm. Eng.* **2018**, *132*, 730−739.
(23) Liu, Z.; Lyu, J.; Fang, D.; Zhang, X. Nanofibrous Kevlar Aerogel Threads for Thermal Insulation in Harsh Environments. *ACS Nano* **2019**, *13*, 5703−5711.
(24) Plappert, S. F.; Nedelec, J.-M.; Rennhofer, H.; Lichtenegger, H. C.; Liebner, F. W. Strain Hardening and Pore Size Harmonization by Uniaxial Densification: A Facile Approach toward Superinsulating Aerogels from Nematic Nanofibrillated 2, 3-Dicarboxyl Cellulose. *Chem. Mater.* **2017**, *29*, 6630−6641.
(25) Kobayashi, Y.; Saito, T.; Isogai, A. Aerogels with 3D Ordered Nanofiber Skeletons of Liquid-crystalline Nanocellulose Derivatives as Tough and Transparent Insulators. *Angew. Chem.* **2014**, *126*, 10562−10565.
(26) Gawryla, M. D.; Schiraldi, D. A. Novel Absorbent Materials Created via Ice Templating. *Macromol. Mater. Eng.* **2009**, *294*, 570−574.
(27) Berglund, L.; Noël, M.; Aitomäki, Y.; Öman, T.; Oksman, K. Production Potential of Cellulose Nanofibers from Industrial Residues: Efficiency and Nanofiber Characteristics. *Ind. Crops Prod.* **2016**, *92*, 84−92.
(28) Saito, T.; Kimura, S.; Nishiyama, Y.; Isogai, A. Cellulose Nanofibers Prepared by TEMPO-Mediated Oxidation of Native Cellulose. *Biomacromolecules* **2007**, *8*, 2485−2491.
(29) Ventura-Cruz, S.; Tecante, A. Extraction and Characterization of Cellulose Nanofibers from Rose Stems (Rosa Spp.). *Carbohydr. Polym.* **2019**, *220*, 53−59.
(30) Hammerschmidt, U. Guarded Hot-Plate (GHP) Method: Uncertainty Assessment. *Int. J. Thermophys.* **2002**, *23*, 1551−1570.
(31) Peng, X.; Zhong, L.; Ren, J.; Sun, R. Laccase and Alkali Treatments of Cellulose Fibre: Surface Lignin and Its Influences on Fibre Surface Properties and Interfacial Behaviour of Sisal Fibre/Phenolic Resin Composites. *Composites, Part A* **2010**, *41*, 1848−1856.
(32) Leite, A. L. M. P.; Zanon, C. D.; Menegalli, F. C. Isolation and Characterization of Cellulose Nanofibers from Cassava Root Bagasse and Peelings. *Carbohydr. Polym.* **2017**, *157*, 962−970.
(33) Xiao, Y.; Liu, Y.; Wang, X.; Li, M.; Lei, H.; Xu, H. Cellulose Nanocrystals Prepared from Wheat Bran: Characterization and Cytotoxicity Assessment. *Int. J. Biol. Macromol.* **2019**, *140*, 225−233.
(34) Azubuike, C. P.; Rodríguez, H.; Okhamafe, A. O.; Rogers, R. D. Physicochemical Properties of Maize Cob Cellulose Powders Reconstituted from Ionic Liquid Solution. *Cellulose* **2012**, *19*, 425−433.
(35) Taheri, H.; Samyn, P. Effect of Homogenization (Microfluidization) Process Parameters in Mechanical Production of Micro- and Nanofibrillated Cellulose on Its Rheological and Morphological Properties. *Cellulose* **2016**, *23*, 1221−1238.
(36) Dos Santos, D. M.; De Lacerda Bukzem, A.; Ascheri, D. P. R.; Signini, R.; De Aquino, G. L. B. Microwave-Assisted Carboxymethylation of Cellulose Extracted from Brewer's Spent Grain. *Carbohydr. Polym.* **2015**, *131*, 125−133.
(37) Di Giorgio, L.; Salgado, P. R.; Dufresne, A.; Mauri, A. N. Nanocelluloses from Phormium (Phormium Tenax) Fibers. *Cellulose* **2020**, *27*, 4975−4990.
(38) Beluns, S.; Gaidukovs, S.; Platnieks, O.; Gaidukova, G.; Mierina, I.; Grase, L.; Starkova, O.; Brazdausks, P.; Thakur, V. K. From Wood and Hemp Biomass Wastes to Sustainable Nanocellulose Foams. *Ind. Crops Prod.* **2021**, *170*, No. 113780.
(39) Matebie, B. Y.; Tizazu, B. Z.; Kadhem, A. A.; Prabhu, S. V. Synthesis of Cellulose Nanocrystals (CNCs) from Brewer's Spent Grain Using Acid Hydrolysis: Characterization and Optimization. *J. Nanomater.* **2021**, *2021*, 1−10.
(40) Song, H. Y.; Park, S. Y.; Kim, S.; Youn, H. J.; Hyun, K. Linear and Nonlinear Oscillatory Rheology of Chemically Pretreated and Non-Pretreated Cellulose Nanofiber Suspensions. *Carbohydr. Polym.* **2022**, *275*, No. 118765.
(41) Dominic, C. D. M.; Raj, V.; Neenu, K. V.; Begum, P. M. S.; Formela, K.; Saeb, M. R.; Prabhu, D. D.; Vijayan, P. P.; Ajithkumar, T. G.; Parameswaranpillai, J. Chlorine-Free Extraction and Structural Characterization of Cellulose Nanofibers from Waste Husk of Millet (Pennisetum Glaucum). *Int. J. Biol. Macromol.* **2022**, *206*, 92−104.
(42) Martins, L. S.; dos Santos, R. G.; Spinacé, M. A. S. Properties of Cellulose Nanofibers Extracted from Eucalyptus and Their Emulsifying Role in the Oil-in-Water Pickering Emulsions. *Waste Biomass Valorization* **2022**, *13*, 689−705.

https://doi.org/10.1021/acssuschemeng.3c01113
ACS Sustainable Chem. Eng. 2023, 11, 10698−10708

(43) Fukuzumi, H.; Saito, T.; Okita, Y.; Isogai, A. Thermal Stabilization of TEMPO-Oxidized Cellulose. *Polym. Degrad. Stab.* **2010**, *95*, 1502−1508.
(44) Mahendra, I. P.; Wirjosentono, B.; Ismail, H.; Mendez, J. A. Thermal and Morphology Properties of Cellulose Nanofiber from TEMPO-Oxidized Lower Part of Empty Fruit Bunches (LEFB). *Open Chem.* **2019**, *17*, 526−536.
(45) Munier, P.; Gordeyeva, K.; Bergström, L.; Fall, A. B. Directional Freezing of Nanocellulose Dispersions Aligns the Rod-like Particles and Produces Low-Density and Robust Particle Networks. *Biomacromolecules* **2016**, *17*, 1875−1881.
(46) Cai, H.; Sharma, S.; Liu, W.; Mu, W.; Liu, W.; Zhang, X.; Deng, Y. Aerogel Microspheres from Natural Cellulose Nanofibrils and Their Application as Cell Culture Scaffold. *Biomacromolecules* **2014**, *15*, 2540−2547.
(47) Gupta, P.; Singh, B.; Agrawal, A. K.; Maji, P. K. Low Density and High Strength Nanofibrillated Cellulose Aerogel for Thermal Insulation Application. *Mater. Des.* **2018**, *158*, 224−236.
(48) Wang, S.; Peng, X.; Zhong, L.; Tan, J.; Jing, S.; Cao, X.; Chen, W.; Liu, C.; Sun, R. An Ultralight, Elastic, Cost-Effective, and Highly Recyclable Superabsorbent from Microfibrillated Cellulose Fibers for Oil Spillage Cleanup. *J. Mater. Chem. A* **2015**, *3*, 8772−8781.
(49) Berglund, L.; Nissila, T.; Sivaraman, D.; Komulainen, S.; Telkki, V.-V.; Oksman, K. Seaweed-Derived Alginate−Cellulose Nanofiber Aerogel for Insulation Applications. *ACS Appl. Mater. Interfaces* **2021**, *13*, 34899−34909.
(50) Zhang, X.; Zhao, X.; Xue, T.; Yang, F.; Fan, W.; Liu, T. Bidirectional Anisotropic Polyimide/Bacterial Cellulose Aerogels by Freeze-Drying for Super-Thermal Insulation. *Chem. Eng. J.* **2020**, *385*, No. 123963.
(51) Zhao, Y.-W.; Tian, M.-Z.; Huang, P. Starch/Clay Aerogel Reinforced by Cellulose Nanofibrils for Thermal Insulation. *Cellulose* **2021**, *28*, 3505−3513.
(52) Tanpichai, S.; Wimolmala, E. Facile Single-Step Preparation of Cellulose Nanofibers by TEMPO-Mediated Oxidation and Their Nanocomposites. *J. Nat. Fibers* **2022**, *19*, 10094−10110.
(53) Cuce, E.; Cuce, P. M.; Wood, C. J.; Riffat, S. B. Toward Aerogel Based Thermal Superinsulation in Buildings: A Comprehensive Review. *Renewable Sustainable Energy Rev.* **2014**, *34*, 273−299.
(54) Antonini, C.; Wu, T.; Zimmermann, T.; Kherbeche, A.; Thoraval, M.-J.; Nyström, G.; Geiger, T. Ultra-Porous Nanocellulose Foams: A Facile and Scalable Fabrication Approach. *Nanomaterials* **2019**, *9*, No. 1142.

https://doi.org/10.1021/acssuschemeng.3c01113
ACS Sustainable Chem. Eng. 2023, 11, 10698−10708